PHYSICAL REVIEW VOLUME 168, NUMBER 3 15 APRIL 1968

Temperature Dependence of Raman and Rayleigh Scattering in $LiNbO_3$ and $LiTaO_3$

W. D. JOHNSTON, JR., AND I. P. KAMINOW
Bell Telephone Laboratories, Holmdel, New Jersey

(Received 1 November 1967)

The Raman spectra of $LiNbO_3$ and $LiTaO_3$ have been investigated between 90 and 1100°K. The dependence of optic-mode frequencies and Raman-scattering efficiencies on temperature indicates that the ferroelectric transition ($T_c \approx 900$°K for $LiTaO_3$, ≈ 1480°K for $LiNbO_3$) is second order and is associated with an optic phonon mode whose frequency becomes small as the Curie temperature is approached from below. Critical Rayleigh scattering is observed for $LiTaO_3$ and the shape of the anomaly is attributed to the combined effects of lattice polarization fluctuation and the discontinuity in electro-optic effect at the transition. The absolute scattering efficiency and linewidth data indicate that the stimulated Raman gain for several lattice modes is comparable with or greater than that for the 655-cm^{-1} CS_2 line, and calculations show that cw Raman oscillation in these modes is feasible.

INTRODUCTION

LITHIUM niobate and lithium tantalate have recently become the subjects of considerable interest because of the large nonlinear optical effects which they exhibit. These isomorphic materials are available as large single crystals of good optical quality[1,2] and are transparent throughout the visible and near infrared. At room temperature, they are ferroelectric with space group $R3c$ (two formula units per unit cell) and have similar lattice constants and ion positions. They differ significantly in other respects, such as Curie temperature T_c(≈ 1485°K for $LiNbO_3$, ≈ 900°K for $LiTaO_3$).

The optic vibrational modes are intimately related to the electro-optic effect as well as to the phase transition to the ferroelectric state. We recently reported the frequency shifts, linewidths, and absolute Raman-scattering efficiencies for the long-wavelength optic phonons in $LiNbO_3$ and $LiTaO_3$ at room temperature, and demonstrated a quantitative relationship between these quantities and the linear electro-optic coefficients.[3] In this paper we describe the principal temperature-dependent features of the optic phonon spectra and discuss these features in terms of current theories of ferroelectricity. We also mention briefly the observation of critical Rayleigh scattering near the Curie point. In addition, the measurements of scattering efficiency and linewidth permit a calculation of available stimulated Raman gain, and this quantity is tabulated for strong modes at different temperatures. In some cases, these gains exceed those reported for any other substance.

BACKGROUND

With 10 ions per unit cell, $LiNbO_3$ and $LiTaO_3$ have 30 degrees of freedom. The symmetry types of the vibrational modes for the low- and high-temperature phases are listed in Table I. The nonzero components of infrared absorption and Raman scattering tensors are also noted. In the ferroelectric phase, 22 optic modes are both Raman- and infrared-active ($4A_1+9E$), and in the paraelectric phase nine of these become Raman- and 13 infrared-active. The macroscopic field produced by the infrared-active phonons raises the degeneracy between longitudinal (L) and transverse (T) modes, thereby doubling the number of observed frequencies for these modes. Above T_c the Raman-active phonons are nonpolar, so that the TL degeneracy is restored and there are only five ($1A_{1g}+4E_g$) characteristic Raman shifts expected.

The above discussion is based on the point-group symmetry ($3m$ below T_c and $\bar{3}m$ above T_c) and is only approximately applicable for the finite-wavelength phonons actually observed. In particular, attention must be restricted to phonons propagating along or perpendicular to the unique crystal (c) axis, since for other directions phonons to not in general possess a well-defined L or T polarization. Even with this restriction, there are additional considerations. For example, a transverse E phonon of finite wavelength can propagate either parallel or perpendicular to the optic axis and may have a different frequency in each case. Similarly, transverse A_1 modes may have different frequencies for propagation along $\langle 010 \rangle$ and $\langle 110 \rangle$. These latter effects, however, were not observed in the present experiment.

The strength of a given Raman-active vibration is given by the scattering efficiency $S/ld\Omega$, where S is the fraction of incident *power* that is scattered into a solid angle $d\Omega$ near a normal to the optical path length l. A semiclassical expression for (Stokes-shifted) scattering efficiency is[4]

$$S_{ij,k}{}^m = \frac{(n_0{}^m+1)\hbar\omega_s{}^4 l d\Omega}{64\pi^2\epsilon_0{}^2 c^4} \frac{|\alpha_{ij,k}{}^m|^2}{\rho^m \omega_m}. \tag{1}$$

---

[1] K. Nassau, H. J. Levinstein, G. M. Loiacono, S. C. Abrahams, J. M. Reddy, J. L. Bernstein, and W. C. Hamilton, J. Phys. Chem. Solids **27**, 983 (1966).

[2] A. A. Ballman, J. Am. Ceram. Soc. **48**, 112 (1965); H. S. Levinstein, A. A. Ballman, and C. D. Capio, J. Appl. Phys. **37**, 4585 (1966).

[3] I. P. Kaminow and W. D. Johnston, Jr., Phys. Rev. **160**, 519 (1967).

[4] M. Born and K. Huang, *Dynamical Theory of Crystal Lattices* (Oxford University Press, London, 1956), p. 199ff.

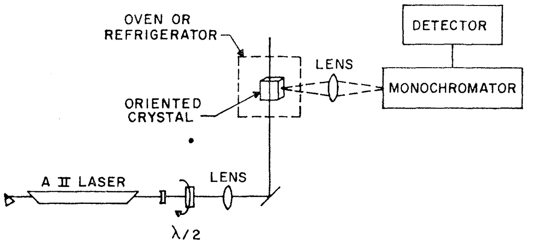

FIG. 1. Experimental arrangement.

Here ϵ_0 is the vacuum permittivity, ω_m is the (circular) frequency of the mth Raman active mode, ω_s is the frequency of the scattered light at the Stokes frequency, n_0^m is the Bose population factor $[\exp(\hbar\omega_m/kT)-1]^{-1}$, ρ^m is an effective reduced mass per unit volume for the mth mode, and $\alpha_{ij,k}$ is the derivative of the optical polarizability per unit volume with respect to the mth normal mode coordinate. Subscripts i and j refer to the polarization directions of scattered and incident photons, and k indicates the symmetry type of the mth mode. For polar modes, k may be referred to the polarization direction ($A_1 \rightarrow z, E \rightarrow \perp z$). A more precise calculation[5] reduces to (1) when ω_m is negligible compared with the photon frequencies.

Finally, we recall the generalized Lyddane-Sachs-Teller (LST) relations[6]

$$\prod_{A_1,A_{2u}} \left(\frac{\omega_m^L}{\omega_m^T}\right)^2 = \frac{\kappa_3}{\kappa_3^\infty}, \qquad \prod_{E,E_u} \left(\frac{\omega_m^L}{\omega_m^T}\right)^2 \frac{\kappa_1}{\kappa_1^\infty}, \tag{2}$$

where $\kappa_{1,3}$ and $\kappa_{1,3}^\infty$ are the low- and high-frequency dielectric constants, and A_{2u} and E_u are the infrared-active modes above T_c. According to the "soft-mode" model[7] of the ferroelectric transition as applied to these materials,[8] the rise in κ_3 as the transition is approached from above is due to a temperature shift of the lowest-frequency A_{2u} transverse mode such that the frequency approaches zero as $(T-T_c)^{1/2}$. The frequencies of the other T and L modes remain approximately constant, as does κ^∞, which is due solely to electronic processes.

Although the soft-mode model was applied originally to the region above T_c, it is clear from (2) and the observed[1] increase in κ_3 as T_c is approached from below that a similar description may apply in this region. There is evidence,[9] which is supported by the present measurements, that the phase transition at T_c is second order, so that $(\kappa_3-1)^{-1}$ is proportional to $T-T_c$ above and to $2(T_c-T)$ below the transition temperature.[10] Hence near T_c the frequency of the lowest A_1 mode should vary continuously as $|T_c-T|^{1/2}$ through T_c. No frequency variations with temperature are expected for other modes. The polar modes of given symmetry type must retain TL alternation along the frequency scale at all temperatures, however, and the T and L branches of a mode that remains Raman-active through T_c must become degenerate in the paraelectric phase.

The Raman intensities of modes that become Raman-inactive at T_c must tend to zero continuously as the transition is approached. In the equation for scattering

TABLE I. Correlation table for optic modes.

$3m(T<T_c)$	$\bar{3}m(T>T_c)$
$4A_1(z;\alpha_{xx}=\alpha_{yy}=a,$ $\alpha_{zz}=b)$	$1A_{1g}(0;\alpha_{xx}=\alpha_{gy}=a',$ $\alpha_{zz}=b'$
	$3A_{2u}(z;0)$
$5A_2(0;0)$	$2A_{1u}(0;0)$
	$3A_{2g}(0;0)$
$9E(x,y;\alpha_{xx}=-\alpha_{yy}=c,$ $\alpha_{xy}=\alpha_{yx}=-c;$ $\alpha_{yz}=\alpha_{zy}=d,$ $\gamma_{xz}=\alpha_{zx}=-d)$	$4E_g(0;\alpha_{xx}=\alpha_{yy}=c',$ $\alpha_{xy}=\alpha_{yz}=-c';$ $\alpha_{yz}=\alpha_{zy}=d',$ $\infty_{xz}=\alpha_{zx}=-d')$
	$5E_u(x,y;0)$

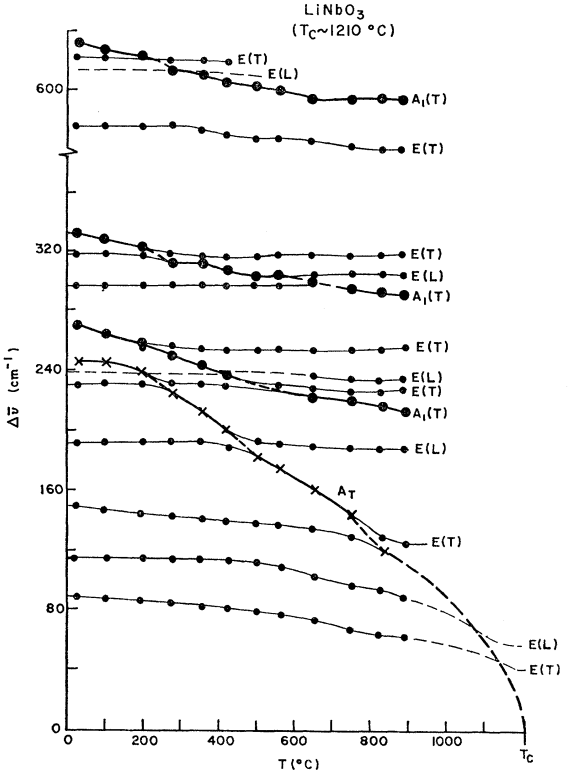

FIG. 2. Temperature dependence of phonon frequency peaks for LiNbO3. Crosses indicate the soft-mode peak.

---

[5] R. Loudon, Advan. Phys. **13**, 423 (1964).

[6] W. Cochran and R. A. Cowley, J. Phys. Chem. Solids **23**, 447 (1962).

[7] W. Cochran, Advan. Phys. **9**, 387 (1960).

[8] A. S. Barker, Jr., and R. Loudon, Phys. Rev. **158**, 433 (1967).

[9] E. G. King and L. B. Pankratz, U. S. Bureau of Mines Report No. 6862, 1966 (unpublished).

[10] F. Jona and G. Shirane, *Ferroelectric Crystals* (The Macmillan Company, New York, 1962), p. 15ff.

efficiency, (1), the quantities that might be temperature-dependent (apart from the Bose factor) are ω_m, ρ^m, and $\alpha_{ij,k}{}^m$. We have assumed ω_m to vary significantly only for the unstable mode. Although the effective mass ρ^m for the mth mode depends not only on the real ionic masses but also, in a crystal of this complexity, on the restoring force constants between ions, it still seems reasonable that ρ^m should not vary appreciably with temperature at least for all but the soft mode. Any temperature variation of the scattering efficiency for these modes is then ascribed to $\alpha_{ij,k}{}^m$. For the soft mode, it may be argued that ρ^m, rather than the effective spring constant, remains invariant as ω_m changes with T because of the simplicity of that mode,[8] i.e., Li and Nb (or Ta) sublattices vibrating along z with a fixed oxygen sublattice.

In order to estimate the form of the temperature variation of scattering efficiency, we expand $\alpha_{ij,k}{}^m$ as a function of P_s, the spontaneous polarization;

$$\alpha_{ij,k}{}^m(P_s)=[\alpha_{ij,k}{}^m]_{P_s=0}+[\partial\alpha_{ij,k}{}^m/\partial P_s]_{P_s=0}P_s+\cdots. \quad (3)$$

At $P_s=0$, the crystals have inversion symmetry and, since $\alpha_{ij,k}$ and $\partial\alpha_{ij,k}/\partial P_s$ are of opposite parity under inversion, one must vanish for any given mode at $P_s=0$. Thus for $T<T_c$ we have, to first order in P_s,

$$\begin{aligned}&\alpha_{ij,k}{}^m(P_s)=\text{const for modes Raman-active above } T_c,\\&\alpha_{ij,k}{}^m(P_s)\sim P_s \text{ for modes Raman-inactive above } T_c. \quad (4)\end{aligned}$$

Since $P_s{}^2\sim(T_c-T)$ for a second-order transition,[10] we have, with the aid of (1) and Table I,

$$\frac{S^m/ld\Omega}{n_0{}^m+1}\sim\begin{cases}\text{const for } 1A_1 \text{ and } 4E \text{ modes}\\ T_c-T \text{ for } 2A_1 \text{ and } 5E \text{ modes}\\ (T_c-T)^{1/2} \text{ for } 1A_1 \text{ ("soft") mode.}\end{cases} \quad (5)$$

EXPERIMENTAL DETAILS

The experimental arrangement is illustrated in Fig. 1. Exciting light (~75 mW) at 4880 Å from an argon ion laser is focused into the sample by the first lens ($f=20$ cm). Light scattered through 90° is collected by the second lens and focussed onto the entrance slit of a double pass, single grating monochromator. The detector consists of an EMI 9502S photomultiplier and a lock-in amplifier referred to a chopper within the monochromator. A half-wave plate $\frac{1}{2}\lambda$ following the laser serves to rotate the incident optical polarization, and a Polaroid polarizer and quarter-wave plate is inserted at the entrance slit of the monochromator.

Samples are typically 4×4×10 mm and are oriented to within 1° by back-reflection Laue x-ray photographs. The crystal cuts employed permit observation of optic phonons with wave vectors along ⟨001⟩, ⟨010⟩, or ⟨110⟩ directions ($z\|c$ axis, $x\perp$ mirror planes, $y\perp x$ and z). For low-temperature (90–300°K) measurements, the samples are mounted in an open cycle N_2 refrigerator. For the temperature range 300–1200°K, the crystals are supported on a thin-walled alumina tube, through which the exciting beam passes, within a magnesia-alumina oven designed to minimize thermal gradients across the sample. Temperatures are monitored by thermocouples in various locations at or near the sample surfaces. Precautions are taken to ensure steady-state thermal conditions during spectral measurements. Since transition temperatures for these materials are known to vary for crystals cut from different boules due to melt stoichiometry variations, no particular effort was made to determine absolute temperatures with high precision. The temperatures indicated in Figs. 2–5, for example, are accurate to about ±3°K.

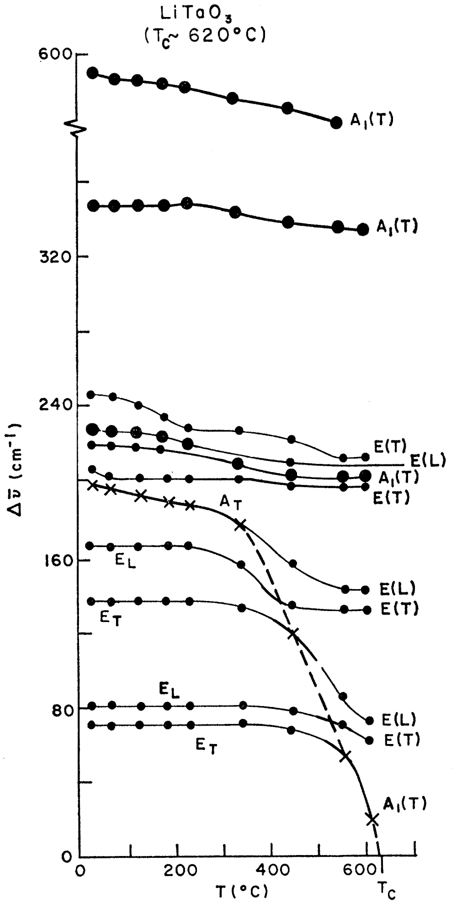

FIG. 3. Temperature dependence of phonon frequency peaks for $LiTaO_3$. Crosses indicate the soft-mode peak.

RAMAN SCATTERING

Frequency Shifts and Scattering Efficiencies

For $LiTaO_3$, observations were made between 90 and 1000°K and include the transition at ≈910°K. For $LiNbO_3$, the transition at ≈1485°K was not observable because the short-wavelength absorption edge moves

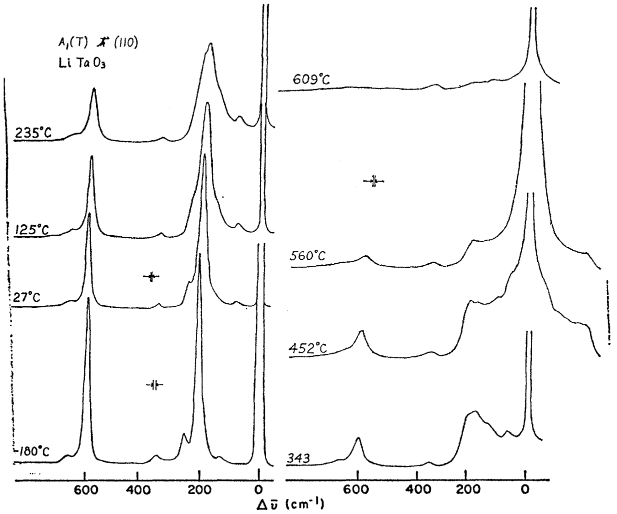

FIG. 4. Stokes spectra for transverse A_1 modes propagating along ⟨110⟩ in LiTaO$_3$ at various temperatures. Incident and scattered light polarized along z.

toward longer wavelengths with increasing temperature, so that at ~1000°K absorption exceeds 40 dB per cm for 4880-Å light. Qualitative measurements were continued to 1100°K with 5145-Å excitation, however.

The observed frequency shifts $\Delta\bar{\nu}$ corresponding to phonons propagating in the ⟨110⟩ direction are plotted against temperature in Figs. 2 and 3. For the sake of clarity, only the lower-frequency E modes are shown in addition to the four A_1 transverse modes. The frequencies of the lowest A_1 transverse mode and the two low-frequency E mode TL pairs shift most strongly. For LiNbO$_3$, the modes are well defined at room temperature and below; and for LiTaO$_3$, at −125°C and below. Unambiguous symmetry-type and polarization assignments can then be made. As the temperature is raised and the frequency of the lowest A_1 mode decreases, the lower E modes mix with the A_1 modes, as may be seen in Fig. 4, where typical spectra are shown for LiTaO$_3$ for incident and scattered photons polarized along z. With this configuration, only four A_1 modes (600, 356, 253, and 201 cm^{-1} at 27°C) should appear. However, additional structure at 648, 163, and 80 cm^{-1} is apparent; these frequencies correspond to modes which also appear as E-type fundamentals. The intensities of the additional modes show no dependence on small deliberate misorientation of the crystal, and the relative intensity of all seven modes remains the same when the collecting lens is stopped down from $f/4$ to $f/32$. Depolarizing effects arising from birefringence[11] should be unimportant because incident and scattered radiation propagate normal to the optic axis. The coupling of A_1 and E phonons is attributed to a temperature-dependent strain perturbation, which effectively lowers the crystal symmetry. Supporting evidence for this contention is summarized in Appendix A.

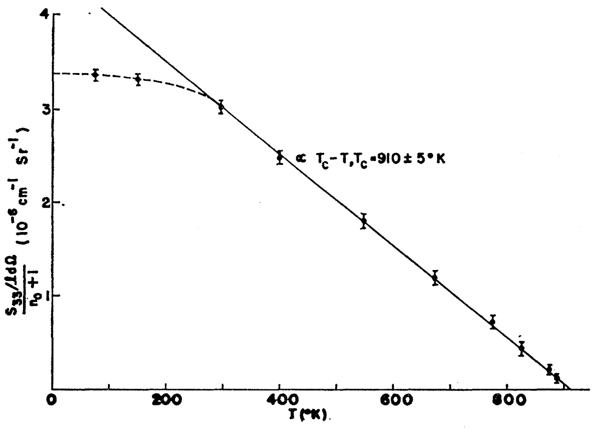

FIG. 5. Scattering efficiency for 600 cm^{-1} (room temperature) A_1 transverse mode in LiTaO$_3$ versus temperature. Solid line proportional to T_c-T.

The mode at 356 cm^{-1} is not perceptibly coupled to nearby E modes, and its intensity is found to be constant (±10%), apart from the Bose factor between 90 and 1000°K. This mode is the only A_1 vibration that remains Raman-active above T_c, and it may be that the absence of strong coupling to E modes is due to the nearly nonpolar character of the mode.

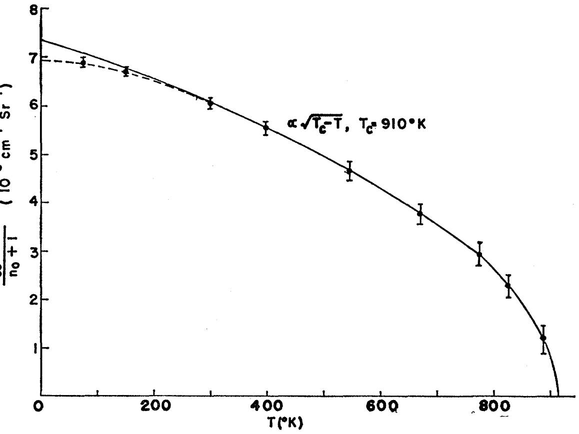

FIG. 6. Scattering efficiency for 200 cm^{-1} (room temperature) "soft" A_1 transverse mode in LiTaO$_3$ versus temperature. Solid curves proportional to $(T_c-T)^{1/2}$.

The mode at 600 cm^{-1} is coupled to E modes at 648 and 596 cm^{-1} at room temperature, and the coupling increases somewhat with increasing temperature. However, the intensity associated with the coupled shoulder at 648 cm^{-1} represents only a small fraction of the total line intensity. The integrated scattering efficiency normalized by the Bose factor for the 600 cm^{-1} A_1 structure is plotted against temperature in Fig. 5. Above 300°K this quantity is linearly proportional to

---

[11] I. P. Kaminow, R. C. C. Leite, and S. P. S. Porto, J. Phys. Chem. Solids 26, 2085 (1965); S. P. S. Porto, J. A. Giordmaine, and T. C. Damen, Phys. Rev. 147, 608 (1966).

$T_c - T$, within the experimental error bars, whether the 648 $\mathrm{cm^{-1}}$ shoulder is included or not. (In order to be consistent with the perturbation approach used in Appendix A the shoulder is included for the data points shown.) The deviation from linearity below 300°K is attributed to polarization saturation. The method used to determine the absolute scattering efficiency is described in Appendix B.

It is clear from Fig. 4 that it is very difficult to follow the soft mode at elevated temperature, much less determine its intensity. However, an indication of the uncoupled intensity of this mode may be obtained by integrating the intensity of the entire low-frequency A_1 (transverse) structure. This quantity is plotted in Fig. 6 and is found to vary as $(T_c - T)^{1/2}$ within measurement accuracy, again apart from the Bose factor. The frequency variation of the Bose factor over the broad line structure is taken into account in the normalization. However, essentially the same results are obtained if the intensity-weighted mean frequency of the soft-mode structure is used at any given temperature. As shown in Fig. 7, this center-of-gravity frequency varies as $(T_c - T)^{1/2}$, which is consistent with (2) and the theoretical[10] and experimental[1,2] behavior of κ_3 near T_c. Again, a slight saturation for both frequency and intensity curves is found at low temperatures. The fact that this curve and the curves in Figs. 2, 3, 5, and 6 appear to extrapolate continuously to the Curie point may be taken as an indication of second-order phase transition.

The data for the $\mathrm{LiNbO_3}$ A_1 phonons are similar to those for $\mathrm{LiTaO_3}$. However, polarization saturation effects persist from low temperatures up to ~400°C for $\mathrm{LiNbO_3}$. Because of the increasing optical absorption above 600°C quantitative intensity measurements were not possible, but the soft-mode mean frequency follows a $(T_c - T)^{1/2}$ law in the range $0.1 \leq T/T_c \leq 0.75$, in which frequency-shift data were obtained.

Linewidths

The absolute scattering efficiencies as well as linewidths at room temperature for all the lines in $\mathrm{LiNbO_3}$ and $\mathrm{LiTaO_3}$ were reported earlier.[3] The measurement technique is discussed in Appendix B. The temperature dependence of widths of the two strongest A_1 transverse lines is plotted in Fig. 8. Scattering efficiences and linewidths at three different temperatures for these lines are tabulated in Table II. The linewidth 2Γ is the full width at half-maximum and the scattering efficiency $S_{33}/ld\Omega$ corresponds to incident and scattered light each polarized along the c axis. Note that the room-temperature linewidths that were quoted earlier[3] are about 30% too small.

The scattering efficiency normalized by the population factor exhibits relatively little variation in the temperature range 90–460°K (see Figs. 5 and 6). The linewidth, on the other hand, decreases substantially with decreasing temperature (see Fig. 8). The rate of decrease is greater for the soft modes, which are broader at room temperature than the higher-frequency lines. A simplified model[5] of line broadening due to anharmonicity predicts a linear dependence on temperature when $\hbar\omega_m/\kappa T \gg 1$ and a temperature-independent width when $\hbar\omega_m/kT \ll 1$. The situation in Fig. 8 and Table II corresponds to an intermediate-temperature region.

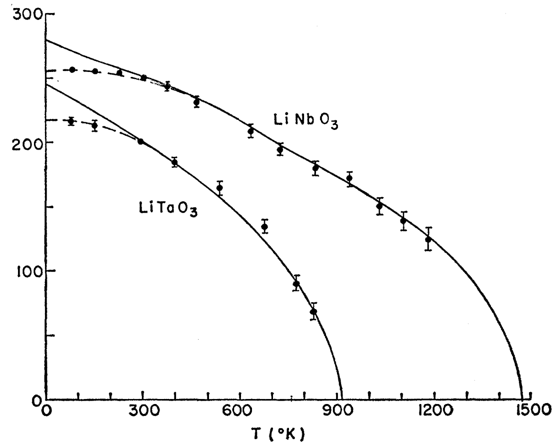

FIG. 7. "Center-of-gravity" frequency of soft mode in LiNbo$_3$ and $\mathrm{LiTaO_3}$ versus temperature. Solid curves proportional to $(T_c - T)^{1/2}$. $T_c(\mathrm{LiTaO_3}) = 910$°K, $T_c(\mathrm{LiNbO_3}) = 1480$°K.

CRITICAL RAYLEIGH SCATTERING

The integrated intensity of Rayleigh scattering observed at 90° in the neighborhood of the Curie point is plotted against temperature for $\mathrm{LiTaO_3}$ in Fig. 9. The symmetric (zz) scattering exhibits an anomaly at T_c, while the off-diagonal (zx) scattering is constant. The measured intensity includes Brillouin-scattered light

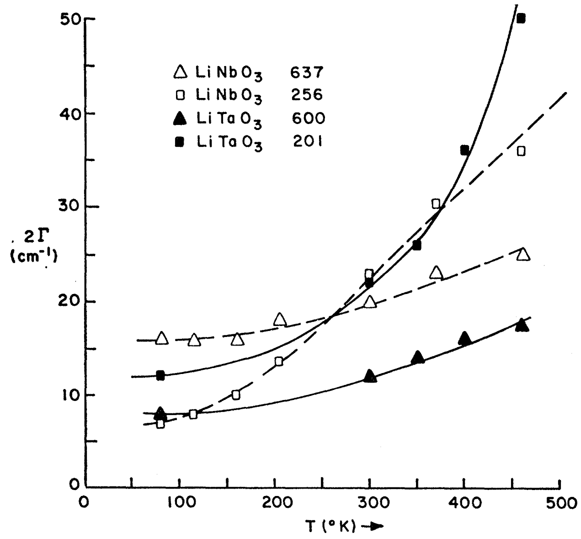

FIG. 8. Full linewidths at half-maximum versus temperature for prominent A_1 transverse modes (identified by room-temperature shifts) in $\mathrm{LiNbO_3}$ and $\mathrm{LiTaO_3}$.

TABLE II. Linewidth, scattering efficiency, and power gain coefficients for $LiTaO_3$ and $LiNbO_3$ at 4880 Å.

		80°K			300°K			400°K		
Material	Line[a]	2Γ (cm^{-1})	$S_{33}/ld\Omega$ (10^{-6} cm^{-1} sr^{-1})	$g_s/(I)$ (10^{-8} cm/W)	2Γ (cm^{-1})	$S_{33}/ld\Omega$ (10^{-6} cm^{-1} sr^{-1})	$g_s/(I)$ (10^{-8} cm/W)	2Γ (cm^{-1})	$S_{33}/ld\Omega$ (10^{-6} cm^{-1} sr^{-1})	$g_s/(I)$ (10^{-8} cm/W)
$LiTaO_3$	201	12	7	2.9	22	10	1.4	50	16	0.8
$LiTaO_3$	600	8	3.2	2.2	12	3.2	1.4	17	2.9	0.8
$LiNbO_3$	256	7	11	8.0	23	16	2.5	36	20	1.6
$LiNbO_3$	637	16	10	3.4	20	10	2.6	25	11	2.0
C_6H_6[b]	992				2.3	0.2	1.2			
CS_2[b]	655				1.4	0.4	2.6			
H_2[c]	4155				...	...	0.3			

[a] Frequency in cm^{-1} at 300°K.
[b] J. G. Skinner and W. G. Nilsen, J. Opt. Soc. Am. **58**, 113 (1968).
[c] N. Bloembergen, G. Bret, P. Lallemand, A. Pine, and P. Simova, IEEE J. Quant. Electron. 3, 197 (1967).

but, as far as possible, does not include low-frequency Raman contributions (see Fig. 4).

The temperature-dependent Rayleigh scattering is caused by nonpropagating fluctuations of the optical dielectric constant that are coupled to a property whose fluctuations have a singularity at T_c. Ginzburg[12] has shown that the variance of polarization fluctuations in a ferroelectric of volume V is

$$\langle \delta P^2 \rangle_{\text{av}} = \epsilon_0(\kappa - 1)kT/V\,, \tag{6}$$

which has the required singularity in the dielectric constant κ. The polarization fluctuations $\langle \delta P^2 \rangle_{\text{av}}$ produce optical dielectric constant fluctuations $\langle \delta\epsilon^2 \rangle_{\text{av}}$ through the linear electro-optic effect below T_c and through the quadratic effect above T_c, where the crystal is centrosymmetric. Since a given $\langle \delta P^2 \rangle_{\text{av}}$ produces a much larger $\langle \delta\epsilon^2 \rangle_{\text{av}}$ by the linear effect than it does by the quadratic effect, the scattered intensity is not expected to resemble the anomaly in $\kappa - 1$. Instead, one expects a discontinuous jump at T_c or an approximation to a jump as indicated in Fig. 9, which resembles the curve predicted by Ginzburg[12] for an "ordinary" second-order transition. The linear electro-optic coefficient involved in the anomalous (zz) scattering is r_{333} (or r_{33}); the linear coefficient that would be involved in (zx) scattering, r_{313} (or r_{53}) vanishes identically by symmetry.

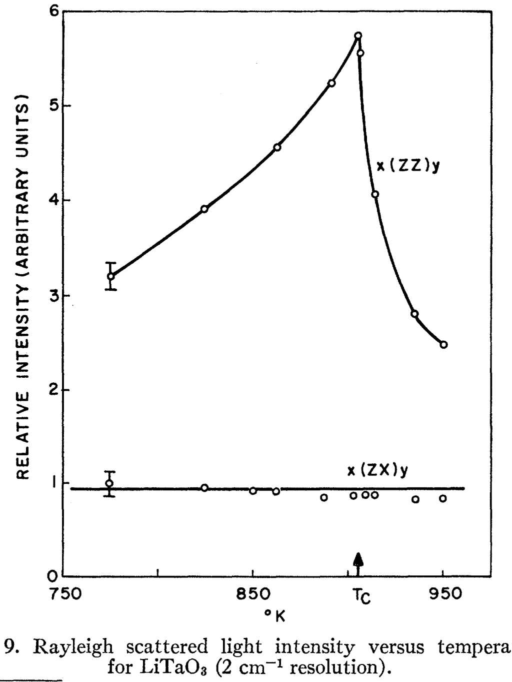

FIG. 9. Rayleigh scattered light intensity versus temperature for $LiTaO_3$ (2 cm^{-1} resolution).

An alternative explanation for the polarization fluctuation near T_c is the formation of static but spatially random microdomains as observed near the $\alpha \leftrightarrow \beta$ transition in quartz.[13] We have not attempted to verify this hypothesis.

STIMULATED RAMAN GAIN

The strong electron-lattice interaction for certain A_1 modes, as indicated by the observed scattering efficiency, is responsible in part for the large lattice contribution to the electro-optic effect.[3] The same interaction manifests itself in large stimulated Raman-gain coefficients for these modes.

The power-gain coefficient for the Stokes wave in MKS units is[14]

$$g_s = \frac{32\pi^2 c^2}{\hbar\omega_s^3} \frac{(S/ld\Omega)(I)}{n_p n_s (n_0+1)(2\Gamma)}\,, \tag{7}$$

where n_p and n_s are refractive indices at the laser and Stokes frequencies, 2Γ is in rad/sec, and the Stokes power increases with length L as $e^{g_s L}$. The coefficient multiplying the laser (or pump) power density I (W/m^2) is tabulated in Table II for $LiTaO_3$ and $LiNbO_3$, as well as for carbon disulphide, benzene, and hydrogen gas. The gain for a given pump power density is greatest for the 256 cm^{-1} $LiNbO_3$ line at 80°K. Further reductions in temperature are not likely to improve the gain because neither $(S/ld\Omega)(n_0+1)^{-1}$ nor the linewidth is changing appreciably near 80°K (see Figs. 6 and 8).

It is clear from (1) and (7) that g_s is proportional to ω_s (far from electronic resonances). The power density

---

[12] V. L. Ginzburg, Usp. Fiz. Nauk *77*, 621 (1962) [English transl.: Soviet Phys.—Usp. **5**, 649 (1963)].

[13] H. Z. Cummins (private communication).

[14] Y. R. Shen and N. Bloembergen, Phys. Rev. **137**, A1787 (1965).

I on the axis of a Gaussian beam[15] containing total power W is $2W/\pi w^2$, where w is the beam radius. If the beam is focussed so that the crystal length L is equal to the confocal parameter, then w^2 is $cL/n_p\omega_p$ at the waist and $2cL/n_p\omega_p$ at the ends. In this situation the total gain g_sL is independent of L and proportional to $\omega_s\omega_p$.

For the 256-cm^{-1} LiNbO$_3$ line at 80°K with a 4880 Å laser, the on-axis gain g_sL is 14×10^{-3} W at the waist, 7×10^{-3} W at the ends, and the average gain is 10^{-2} W. For a laser pump at 1.06 μ, g_sL is reduced by a factor of 4.7. If a confocal resonator is provided for the Stokes frequency (transparent at the laser frequency), sufficient laser power must be provided to produce net gain over a sizeable beam radius if diffraction losses and mode conversion are to be kept small. If we take this characteristic radius to be the point at which g_sL is $1/e$ the on-axis gain, i.e., $r=w/\sqrt{2}$, then g_sL is greater than 0.05 over this radius for 14 W at 4880 Å or 64 W at 1.06 μ.

Although Raman amplification is a parametric process, the Raman gains quoted above for LiNbO$_3$ are considerably smaller than those found for pure electronic parametric gain.[16] The parametric power gain coefficient is

$$g_p=\left(\frac{d^2\omega_s\omega_i I}{2n_pn_sn_i\epsilon_0{}^3c^3}\right)^{1/2}, \tag{8}$$

where d is a nonlinear coefficient, and ω_s and ω_i are the signal and idler frequencies. Roughly speaking, the Raman-gain coefficient is the square of the parametric coefficient. Inasmuch as the gain coefficients are typically less than unity for realizeable power densities, g_p is normally greater than g_s even though the equivalent nonlinear interaction may be greater for the Raman case. The nonlinearity in the Raman case is larger because one of the parametric frequencies coincides with a resonance of the system. For the same reason, the losses at that frequency—the idler frequency—are much greater than the parametric gain, so that only the signal (Stokes) frequency grows. The lack of a growing idler, then, accounts for the second-order appearance of (7) as compared with (8).

Despite its smaller gain, the Raman oscillator has certain advantages over the parametric device: (a) The optical phonon frequency is practically independent of wave vector in the region of interest, so that velocity matching may be achieved at any temperature, with any combination of refractive indices for light propagation along a principal axis. (b) Since vibrational frequency losses are large, there is no need to provide simultaneous resonance[16] in the optical resonator at both signal and idler frequencies. (c) The Stokes frequency is determined by the laser and vibrational frequencies. The vibrational frequency can, in principle, be adjusted continuously by the application of electric fields or mechanical stresses, by temperature changes, or by orientation of the crystal with respect to the laser so as to operate in the polariton region. (d) Unlike the electronic parametric oscillator in a cavity simultaneously resonant for signal and idler, the Raman oscillator does not require a single-mode laser pump.[17] The vibrational linewidth usually exceeds the range over which a multimode laser can oscillate. Each laser mode can then mix with the vibrational resonance at a frequency which contributes to a single Stokes mode in the optical resonator. Whether one or more resonator modes approach threshold will depend on the selectivity of g_s, the pump power, and the resonator mode spacing. If a number of resonator modes should have similar thresholds, one will always dominate and grow at the expense of the others.

CONCLUSIONS

We have examined the behavior of the Raman spectra of LiTaO$_3$ and LiNbO$_3$ as the Curie temperature is approached from the ferroelectric region and find that a particular vibrational mode approaches zero frequency in the neighborhood of the transition. Such soft-mode behavior is similar to that found in other experiments where the transition is approached from above.[18] In either case, with a knowledge of the temperature dependence of dielectric constant, the effect may be regarded as a consequence of the LST relations. These relations, however, do not predict that only one vibrational mode will dominate the transition although such behavior seems quite reasonable.

The shape of the Rayleigh-scattering anomaly in LiTaO$_3$ is attributed to the combined effects of lattice-polarization fluctuations and refractive-index fluctuations induced by them through the linear and quadratic electro-optic effects below and above T_c, respectively. Measurements of the electro-optic effects near the transition as well as absolute scattering intensity measurements could lead to a better understanding of the critical scattering process.

Materials with large Raman-scattering efficiencies and narrow linewidths are interesting candidates for use in Raman oscillators. The present results indicate that LiNbO$_3$ at liquid-nitrogen temperature can be made to oscillate with available laser pumps, at least on a pulsed basis. In addition to its technical interest as an oscillator at the Stokes frequency, such a device might be a useful far-infrared source at the vibrational frequency.

The electro-optic effect in LiNbO$_3$ and LiTaO$_3$ is due largely to an electron-lattice interaction for a single vibrational mode that can be excited by an external

---

[15] H. Kogelnik and T. Li, Proc. IEEE **54**, 1312 (1966).

[16] G. D. Boyd and A. Ashkin, Phys. Rev. **146**, 187 (1966).

[17] S. E. Harris, IEEE J. Quant. Electron **2**, 701 (1966).

[18] A. S. Barker, Jr., in *Ferroelectricity*, edited by E. F. Weller (Elsevier Publishing Co., New York, 1967).

electric field.[3] The electro-optic coefficient is proportional to the square root of the product of scattering efficiency and infrared oscillator strength divided by $\omega_m(n_0+1)$. Measurements[19] of the r_{33} coefficient in $LiTaO_3$ up to 200°C show an increase with temperature. Both S_{33} and ω_m decrease as the temperature approaches T_c while the dielectric constant, which may be taken as an indicator of oscillator strength, increases[2] in such a way as to give an increasing r_{33}. However, the quantitative correlation between measured and calculated r_{33} is not conclusive because of the lack of infrared data and because of the narrow temperature range of the available electro-optic data.

It may be noted at this point that a correlation between electro-optic coefficients and Raman and infrared strengths can also be made above the ferroelectric transition, where the electro-optic effect is quadratic. In the quadratic case, a particular mode cannot be both Raman- and infrared-active in first order. The electro-optic contribution of a mode is given by a term proportional to the product of the first-order Raman efficiency and second-order infrared strength or the product of second-order Raman and the square of the first-order infrared strengths.

ACKNOWLEDGMENTS

We are grateful to A. A. Ballman and K. Nassau, who provided the crystals used in the experiment.

APPENDIX A: STRAIN EFFECTS AND A_1-E MODE COUPLING

The additional structure beyond the four permitted fundamentals in the transverse A_1 spectrum for both $LiNbO_3$ and $LiTaO_3$ is attributed to strains, which relax the selection rules for nominally E-type fundamentals. Supporting evidence is (a) All the additional structure coincides with modes seen prominently in allowed E-type Raman and infrared spectra; (b) the Stokes/anti-Stokes intensity ratios for the additional structure in A_1 spectra vary with temperature in a manner consistent with single phonon (rather than sum or difference) processes; and (c) as noted below, strains of the appropriate symmetry to cause A_1-E mixing are indeed present in our samples to an extent that correlates with the observed breakdown of selection rules.

TABLE III. Correlation between strain and A_1-E mode mixing in $x(zz)y$ scattering at 300°K.

Sample	n_x-n_y	Intensity ratio forbidden/allowed modes
$LiNbO_3$ 1	$<0.6\times10^{-7}$	$<0.1\times10^{-2}$
2	2.6×10^{-7}	0.5×10^{-2}
$LiTaO_3$ 1	$11\ \times10^{-7}$	$20\ \times10^{-3}$
2	$19\ \times10^{-7}$	$38\ \times10^{-3}$

We adopt the perturbation approach used by Barker.[20] From the multiplication properties of the $3m$ character table, it may be shown that for an E mode to become Raman-active for (zz) incident and scattered photon polarization, the strain must contain a term transforming like E. The four strain components with this property are $(\epsilon_1-\epsilon_2)$, ϵ_4, ϵ_5, and ϵ_6. ($\epsilon_1+\epsilon_2$ and ϵ_3 transform like the totally symmetric representation A_1 and do not cause mode mixing.)

The presence of strain was confirmed by measuring the birefringence n_x-n_y for light propagating along the optic axis of two $LiNbO_3$ and two $LiTaO_3$ samples, using a polarizing microscope and quartz compensator. For this condition we have

$$\begin{aligned} n_x-n_y &= n^0+\delta n_x-(n^0+\delta n_y)\,, \\ &= \delta n_x-\delta n_y\,. \end{aligned} \tag{A1}$$

For point group[21] $3m$ we obtain

$$n_x-n_y=-\tfrac{1}{2}(n^0)^3[(p_{11}-p_{12})(\epsilon_1-\epsilon_2)+2p_{14}\epsilon_4]\,, \tag{A2}$$

where p_{ij} are the photoelastic tensor elements.[22] Hence nonzero birefringence n_x-n_y implies nonzero ϵ_4 and/or $\epsilon_1-\epsilon_2$ strain components, each of which can mix A_1 and E modes. In Table III, the values of n_x-n_y measured at room temperature are compared with the ratio of intensities of forbidden and allowed modes in $y(zz)x$ Raman spectra. Definite correlation is apparent. The strain birefringence measured did not vary significantly throughout the volume of any sample save within $\approx 50\ \mu$ of the edges. The (zz) "forbidden" Raman intensities were similarly independent of location of the laser beam within the samples, or the degree of focusing of the beam. Since the samples were all poled and known to be single domain from pyroelectric and electro-optic measurements, domain walls should not be a source of the strain. Presumably the strain arises from "grown-in" imperfections, e.g., dislocations or defects (possibly oxygen vacancies).

APPENDIX B: DETERMINATION OF SCATTERING EFFICIENCY AND LINEWIDTH

The following treatment shows how the absolute scattering efficiencies and linewidths may be determined from observed Raman spectra by comparison with the spectrum of benzene or other substance, for which the scattering efficiency and linewidth have been determined by other means.[23]

Let $P(\omega)d\omega$ be the scattered power in the frequency interval $d\omega$ for a particular Raman line for a given incident power W, path length l, and solid angle $d\Omega$.

---

[19] E. H. Turner (unpublished).

[20] A. S. Barker, Jr., Phys. Rev. **132**, 1474 (1963).

[21] J. F. Nye, *Physical Properties of Crystals* (Oxford University Press, London, 1964).

[22] Six of these have been measured for $LiNbO_3$; see R. G. Dixon and M. G. Cohen, Appl. Phys. Letters **8**, 205 (1966).

[23] J. G. Skinner and W. G. Nilsen, J. Opt. Soc. Am. **58**, 113 (1968).

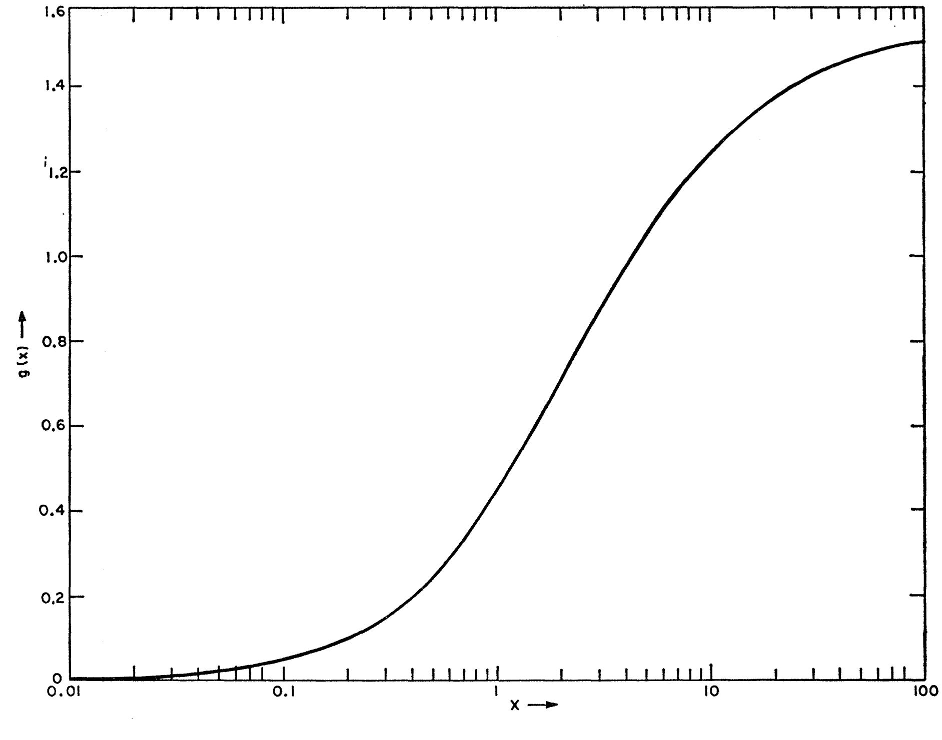

FIG. 10. Plot of $g(x)=\tan^{-1}x-(1/2x)\ln(1+x^2)$.

The response of the spectrometer detection system to a unit frequency impulse excitation $\delta(\omega')$ is a triangle function[24] when diffraction effects are negligible and the entrance and exit slits are identical. The triangle function $t\,(x-x')$, with base $2b$ and height h is centered at the spectrometer recorder position x' corresponding to frequency ω' and vanishes for $|x-x'|>b$. For arbitrary excitation the area A under the spectrometer response function $T(x)$ is

$$A=\int_0^\infty T(x)dx=\int_0^\infty\int_0^\infty P(x')t(x-x')dx'dx$$
$$=W\tau, \tag{B1}$$

where

$$\tau=\int_0^\infty t(x-x')dx=bh, \tag{B2}$$

for $x'>b$, and $\hat{W}$ is the integrated power in the scattered line,

$$\hat{W}=\int_0^\infty P(\omega')d\omega. \tag{B3}$$

The scattering efficiency is

$$S/ld\Omega=\hat{W}/Wld\Omega. \tag{B4}$$

Thus, if the efficiency of a line of a particular substance is known (e.g., the 992-cm^{-1} line in benzene[23]), the *efficiency* of any other line may be determined from

$$S/ld\Omega=\frac{\gamma_B A W_B(ld\Omega)_B}{\gamma A_B W(ld\Omega)}\left(\frac{S}{ld\Omega}\right)_B, \tag{B5}$$

where the subscript B refers to the known substance and γ_B/γ is the ratio of instrument sensitivity in the neighborhood of the known and unknown lines. The sensitivity ratio can be determined with the aid of a calibrated black-body source. It is assumed that all spectrometer adjustments are identical for both the known and unknown spectra. Variation in reflectivity and solid angle due to refractive-index differences in the substances can be taken into account in a straightforward manner.

In order to determine the *width* of an unknown line using the width of a previously measured line, the line is assumed to have the Lorentzian form

$$P(\omega)=P(\omega_0)\Gamma^2/[(\omega_0-\omega)^2+\Gamma^2], \tag{B6}$$

where Γ is the half-width at half-maximum and $\Gamma\ll\omega_0$. Then the recorder response at the resonance frequency ω_0 is

$$T(x_0)=\gamma\int_0^\infty P(\omega')t(x_0-x')dx$$
$$=2h\gamma P(\omega_0)\Gamma g(b/\Gamma), \tag{B7}$$

where

$$g(b/\Gamma)=\tan^{-1}b/\Gamma-(\Gamma/2b)\ln(1+b^2/\Gamma^2). \tag{B8}$$

The quantity b is determined from the triangular response to excitation by light scattered directly from the

---

[24] V. Z. Williams, Rev. Sci. Instr. **19**, 135 (1948); A. Roseler, Infrared Phys. **6**, 111 (1966).

laser. Comparing parameters for the known and unknown lines, we have

$$\frac{T(\omega_0)}{T(\omega_0{}^B)}=\frac{\gamma P(\omega_0)\Gamma g(b/\Gamma)}{\gamma_B P(\omega_0{}^B)\Gamma_B g(b/\Gamma_B)}. \tag{B9}$$

But, with Eqs. (6) and (1),

$$W=\pi P(\omega_0)\Gamma=A/\gamma t, \tag{B10}$$

and

$$g\left(\frac{b}{\Gamma}\right)=\frac{T(\omega_0)A_B}{T_B(\omega_0{}^B)A}g\left(\frac{b}{\Gamma_B}\right), \tag{B11}$$

from which Γ may be determined with the aid of the plot of $g(b/\Gamma)$ in Fig. 10. It is not necessary to use a calibrated substance to find Γ since the laser line itself may be used as the reference in (11) with $b/\Gamma_B \rightarrow \infty$ and $g(\infty)=\frac{1}{2}\pi$. When the recorder response function $T(\omega)$ is similar in form for both the known and unknown lines, then

$$A_B A=T_B(\omega_0{}^B)D_B T(\omega_0)D, \tag{B12}$$

where D is some appropriately chosen linewidth for the recorded spectrum, and (11) can be simplified accordingly.

The greatest source of error is in the determination of the appropriate areas under the spectra in the presence of noise and nearby lines. At best, the absolute accuracy of our measurements probably does not exceed 5% for the strongest modes, with 10% being more typical.

PHYSICAL REVIEW VOLUME 168, NUMBER 3 15 APRIL 1968

Lattice Dynamics and Second-Order Raman Spectrum of CsF†

JOHN R. HARDY* AND ARNOLD M. KARO
Lawrence Radiation Laboratory, University of California, Livermore, California

(Received 16 October 1967)

Results are presented for a precise calculation, based on the deformation dipole model with short-range repulsive interactions between second-neighbor negative ions, of the normal-mode frequency distribution of CsF. The extreme properties of this crystal are reflected in the unusual appearance of the distribution. From these results, we can also predict the form of the second-order Raman spectrum of CsF for two alternative assumptions regarding the Raman polarizability tensor. Both spectra are unusual in that they consist almost entirely of very sharp, clearly separated lines. Furthermore, the spectra corresponding to these two assumptions are very different and should be easily distinguishable experimentally.

SOME time ago we presented the results of a systematic investigation into the lattice dynamics of most of the NaCl-structure alkali halides.[1] However, certain salts were omitted from this initial study, mainly because of the absence of the required input data, and among these was CsF. This was unfortunate since this compound is, in many respects, an extreme case, with the positive ion being both very much heavier and considerably more polarizable than the negative ion. Since that time, sufficient experimental data[2] have become available for us to be able to treat this crystal, and we wish to report in this paper the results of our calculations. Also we wish to report the results of an associated calculation of the second-order Raman spectrum of this crystal. We believe that these calculations will be of direct and immediate interest to experimental workers studying phonon-assisted electronic transitions at defect centers in CsF, defect vibrations in CsF, and the second-order Raman spectrum of CsF. In the first place, apart from a much earlier calculation by one of us (A. M. K.),[3] there is no other theoretical work on the lattice dynamics of CsF. In the second place, our present work has revealed that the extreme properties of CsF are reflected both in the calculated frequency spectrum and the calculated second-order Raman spectrum. Both of these have a very striking appearance which should be well worth investigation by any, or all, of the experimental techniques mentioned above.

The calculations presented here were carried out within the framework of the deformation dipole (DD) model which is fully described in an earlier paper.[4] However, we have recently made an investigation into the Debye-Waller factors of all the cesium halides,[5] including CsF, and we have found it necessary, particularly for CsF, to include short-range interactions between second-neighbor negative ions to obtain good agreement with experiment (i.e., within the quoted

---

† Work performed under the auspices of the U. S. Atomic Energy Commission.

* Permanent address: Behlen Laboratory of Physics, University of Nebraska, Lincoln, Neb.

[1] A. M. Karo and J. R. Hardy, Phys. Rev. **129**, 2024 (1963).

[2] C. M. Randall, R. M. Fuller, and D. J. Montgomery, Solid State Commun. **2**, 273 (1964).

[3] A. M. Karo, J. Chem. Phys. **33**, 7 (1960).

[4] J. R. Hardy, Phil. Mag. **7**, 315 (1962).

[5] A. M. Karo and J. R. Hardy (to be published).